KFUPM
Journal of Undergraduate Research International

Diamond Open Access

Article

Bioengineering

Computational Investigation of Continuum-Like Behavior in Segmented Beam Structures with Frictional Interfaces

Mohannad F. Al Sindhi and Ahmed S. Dalaq*

Cite https://doi.org/10.64589/juri/221332

Submitted: December 02, 2025 **Revised:** March 22, 2026 **Accepted:** March 30, 2026

ABSTRACT

The prevalence and consistency of segmented materials in nature have resulted in increased research attention aiming to use them to produce tough materials from brittle and fragile basic constituents. Therefore, studies have been conducted to determine the underlying mechanics of segmented materials. Some investigators argue that segmented configurations are better described as engineered structures rather than materials because their properties arise from geometry and assembly rather than intrinsic composition. In this study, a computational model was developed to predict the kinematics and kinetics of an array of linear elastic blocks that form a beam under a transverse load, in which the blocks interact via contact and dry friction. The model was experimentally validated and used to explore the design space characterized by the number of blocks and friction coefficient between them. The results showed that the mechanical response increased with increasing friction akin to block fusion, and with an increasing number of blocks analogous to the separation of the scale argument of periodic materials. The increase in friction coefficient from 0.2 to 1.0 improved strength by up to $6\times$ at low N ($N = 3$), without changing the deformation modes. Although increasing f and N induced a transition in the deformation mode to "hinging," with strength increasing by up to $3\times$ (e.g., at $N = 7, f = 1.0$), competition with the increased compliance associated with higher N remains. These findings show that increasing friction or block number promotes the transition of segmented structures toward continuum-like behavior, offering insight into the design of architectured materials with tunable properties.

Keywords: segmented beam structures, topologically interlocked materials, continuum-like behavior, frictional contact mechanics, finite element modeling, structural mechanics

1. INTRODUCTION

In biology, segmentation, also known as metamerism, refers to repeated structural units along a body axis. Multicellular animals and plants commonly exhibit such repetition, for example, in limbs[1]. Segmentation spans multiple length scales and includes the fundamental structural system of animals, the skeleton.

Natural structural materials, such as bone, teeth, and mollusk shells, consist of stiff building blocks of defined sizes and shapes arranged in periodic patterns. Their mechanical performance arises from the interplay between their building block properties, geometry, and arrangement[4]. Notable examples are the tesserae in sharks (Lamna nasus)[2] (Fig. 1a, b) and intervertebral columns (Fig. 1a, c), which form a segmented series of robust blocks optimized for flexibility and load bearing. In species such as sharks and aquatic mammals, this design enables the spine to act as either a spring or a brake, depending on swimming requirements[5–8].

Biological examples have inspired engineered segmented materials, in which patterned elastic (relatively rigid) blocks are set to interlock, slide, or rotate to produce tuneable mechanical responses[6]. Segmented structures form the basis of topologically interlocked materials (TIMs), which are assemblies in which blocks are secured to one another (i.e., maintain static stability) through geometry and edge abutments. The load is transmitted through friction and contact, resulting in ductility and tunable strength[4,6–8]. Topological interlocking combines the damage tolerance of fragmented assemblies with the overall structural integrity of a continuous structure[9–14].

Segmentation or fragmentation improves strength by allowing arrest at interfaces and maintaining stability, even when some blocks fail[15,16]. By tailoring the geometry and interfaces, TIMs can achieve combinations of properties rarely found in monolithic materials, including simultaneous strength and toughness and high resistance to impact[9,15,17,18]. Their mechanical responses are governed by block interactions, which are often studied using load-line analysis, finite element methods, or discrete element methods. Distributed deformation and delayed strain localization increase toughness and resistance to damage[15,19–23]. Although TIMs can initially be less stiff because the blocks can move relative to one another, they are much tougher than brittle solids. Some TIMs also exhibit mechanical chirality[26], and hollow blocks do not compromise their performance[21,25].

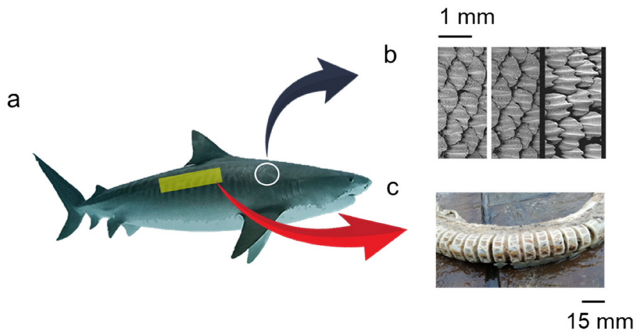

Figure 1. Segmentation in nature. (a) Shark (Lamna nasus), (b) tesserae in shark skin (Lamna nasus), adapted from [2], and (c) part of the shark's intervertebral column, which forms a cartilaginous segmented column, adapted from [3]

Despite extensive research on TIMs and, segmented or fragmented beams and panels, the connection between fragmentation and TIMs remains unclear. TIMs are designed to behave as tough materials; however, fragmentation often gives rise to structures rather than materials. Studies typically consider these systems separately; therefore, it is difficult to establish a unified understanding of how segmented or fragmented structures, such as masonry, relate to fragmented materials. However, the relationship between segmented structures and topologically interlocked materials remains insufficiently understood, particularly in terms of when a segmented assembly begins to exhibit continuum-like behavior. Existing studies typically treat these systems independently, and a clear framework linking discrete structural response to material-like behavior is lacking. This gap limits the ability to rationally design segmented systems with predictable and tunable mechanical properties. Understanding whether increasing the number of blocks in a segmented structure causes it to behave as a material is crucial. To address this, we progressively increased the block count and friction between blocks to determine when a segmented assembly begins to exhibit material-like behavior. We used a simple quasi-static finite element model with dry contact mechanics enforced at the interfaces between different elastic domains. These elastic domains represent the blocks that interact within a fragmented beam. The finite element model was first validated against experimental results from the literature and then used to identify the point at which a segmented structure transitions into a continuum (i.e., a material). In this work, we focused on a fragmented beam, which provides a tractable base model for investigating the distinction between segmentation and fragmentation and for identifying the thresholds at which a structure transitions into a material.

2. METHODOLOGY

2.1. Computational Model.

The segmented beam comprised N linearly elastic blocks in an array configuration. Each block forms a standalone elastic domain governed by the equilibrium equation [26]

$$\frac{\partial \sigma_{xx}}{\partial x} + \frac{\partial \sigma_{xy}}{\partial y} = 0, \qquad \frac{\partial \sigma_{xy}}{\partial x} + \frac{\partial \sigma_{yy}}{\partial y} = 0. \tag{1}$$

Where σ_{xx}, σ_{xy}, and σ_{yy} are the stress tensor components in the 2D domain. We assume a plane-strain case with the following constitutive law (Fig. 2) [26]:

$$\begin{aligned} \sigma_{xx} &= (\lambda + 2\mu)\,\varepsilon_{xx} + \lambda \varepsilon_{yy} \\ \sigma_{yy} &= \lambda \varepsilon_{xx} + (\lambda + 2\mu)\,\varepsilon_{yy} \\ \sigma_{xy} &= 2\mu \varepsilon_{xy}. \end{aligned} \tag{2}$$

Where the strains are:

$$\varepsilon_{xx} = \frac{\partial u}{\partial x}, \quad \varepsilon_{yy} = \frac{\partial v}{\partial y}, \quad \varepsilon_{xy} = \frac{1}{2}\left(\frac{\partial u}{\partial y} + \frac{\partial v}{\partial x}\right). \tag{3}$$

where u and v are the components of the displacement vector along the x and y directions, respectively.

The contact interfaces were defined at the boundaries between all elastic blocks (see the red interfaces in Fig. 2). Contact was enforced using an augmented Lagrangian algorithm [27]. Coulombic friction was considered for the frictional interaction between the blocks [5]. Other boundary conditions included a fixed displacement in the vertical direction along the vertical sides of the segmented beam (see blue domain Ω), which can be expressed as follows (Fig. 2):

$$v(\mathbf{x}) = 0 \text{ for} \tag{4}$$

$$u(\mathbf{x}) = \pm\Delta \text{ for } \mathbf{x} \in \Omega \tag{5}$$

where $\mathbf{x}$ denotes the position vector. The horizontal abutment support on which the segmented beam rests provides vertical support (black domain in Fig. 2).

$$v(\mathbf{x}) = 0 \text{ for} \tag{6}$$

The central block located at $\left(x = NL/2,\ y = L/2\right)$ is subjected to transverse displacement (red arrow in Fig. 2).

$$v(x = NL/2, y = L/2) = -L \tag{7}$$

This boundary value problem was solved using COMSOL Multiphysics [28] with pseudo-increments until the model stopped converging owing to the loss of stability or high nonlinearity arising from the contact interaction. Quadratic quadrilateral elements were also used.

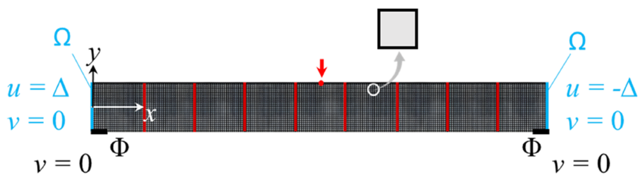

Figure 2. Meshed elastic domain and numerical problem setup, showing the applied boundary conditions. The gray regions represent the elastic blocks forming the segmented beam, with red vertical lines indicating contact interfaces between adjacent blocks. Blue symbols (Ω) denote the constrained boundary regions at both ends, while Φ symbols indicate horizontal abutment supports. Prescribed displacements include $u = \pm\Delta$ and $v = 0$. The white and red arrows indicate the directions of axial loading and applied transverse displacement, respectively, while the curved gray arrow illustrates the resulting rotation of the central block. A sample element is enlarged for demonstration.

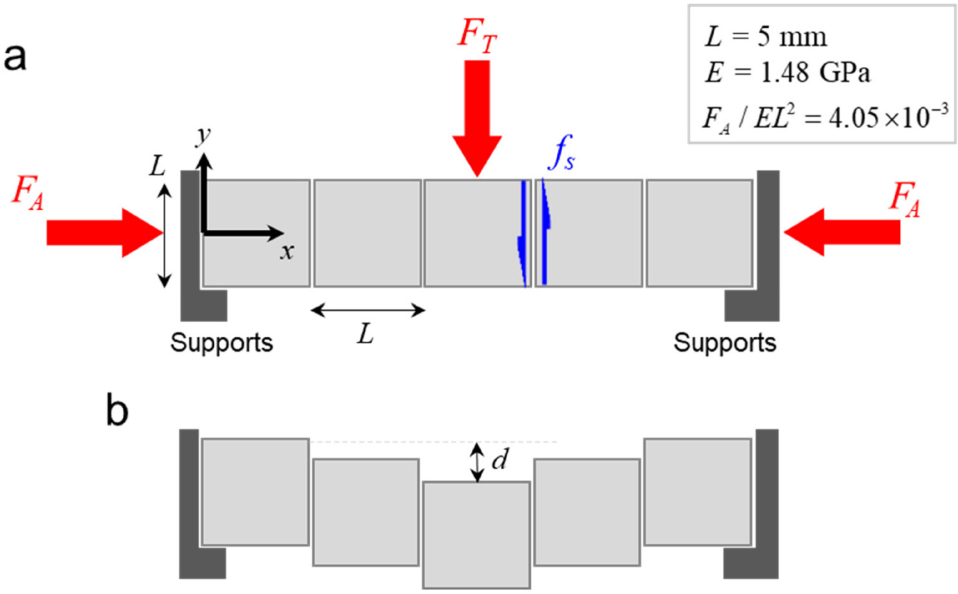

Figure 3. (a) Schematic of the segmented beam subjected to an axial load F_A and a transverse load F_T. (b) Deformed configuration of the segmented beam showing a transverse deflection d.

3. RESULTS AND DISCUSSION

3.1. Segmented Beam Structure. In this section, we introduce the concept of a segmented beam. In this study, we focused on presenting a segmented beam because beam mechanics are well established, and any distinctions that emerge from segmentation would reveal interesting underlying behaviors inherent to the segmented architecture [5].

An array of N identical elastic blocks was considered, each made from an ABS-like material with a Young's modulus $E =$ 1.48 GPa and Poisson's ratio $\nu = 0.3$ (Fig. 3a). This study considered only an odd number of blocks. Each block has a length of $L = 5$ mm. To ensure mechanical interaction and static equilibrium among the blocks, we subjected their lateral faces to an axial pre-stress of $F_A/EL^2 = 4.05 \times 10^{-3}$. The blocks rested on the rigid abutments of height 0.1 L.

When a transverse load FT is applied to the central block located at $x = NL/2$, the block undergoes a vertical downward displacement. The model accounts for dry contact interactions between adjacent blocks through frictional contact (governed by the friction coefficient f) and normal contact enforcement, implemented via an augmented Lagrangian algorithm. We assume here that the dynamic friction is equivalent to static friction, i.e., $f_s = f_d = f$. Two intersecting surfaces with concomitant stresses are subjected to localized shear stress, τ, and only when τ exceeds the local normal interfacial strength, $\tau \geq f\sigma$, where σ is the localized compressive stress, does slip initiate. At that instant, crack-like behavior ensued and localized slip occurred, which tended to depend on the static friction coefficient. Upon movement of the blocks relative to each other, the localized strength decreased slightly, and the dynamic friction coefficient was used. Assuming that equal static and dynamic friction coefficients are associated with a less catastrophic onset of sliding, the interfaces were not too brittle.

Consequently, the displaced block interacts with its neighbors and may drag adjacent blocks either via sliding or hinging [5]. As such, the blocks are deflected by d (Fig. 3b). The overall motion of the array, that is, block translations, local deformations, and rotations, is governed by the parameters F_A/EL^2, $N, f,$ *and* L. In this study, E and L were fixed, as described above. The objective of this work was to understand the effect of the parameters N and f on the global kinematics of the segmented beam and on the resulting force–deflection response $FT-d$.

The elastic domain, which comprises the square block domain, is governed by equilibrium equations. Numerically, we imposed a displacement-driven problem, in which displacements are applied at the central block $(x = NL/2,\ y = L/2)$. The contact was enforced using an augmented Lagrangian method. To solve this contact-based boundary value problem under static conditions with no inertial terms, we used COMSOL Multiphysics [28]. The axial force F_A was applied at $x = 0$ and $x = NL$ and was maintained constant using pseudo increments of the solver. The reaction forces were summed at the location where the transverse displacement was applied (i.e., $x = NL/2,\ y = L/2$). See Methods for further details.

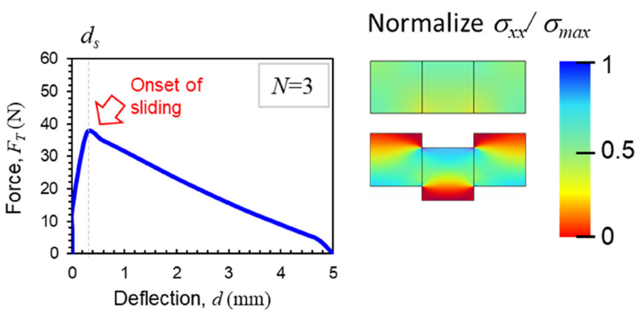

Figure 4. $F_T - d$ response for the case $N = 3$. The corresponding block deformation owing to sliding and the normalized axial stress distribution are shown adjacent to the plot at $d = 1.5$ mm.

3.2. Transverse Response. Figure 4 shows the transverse responses of the three blocks. The force–deflection curve exhibits

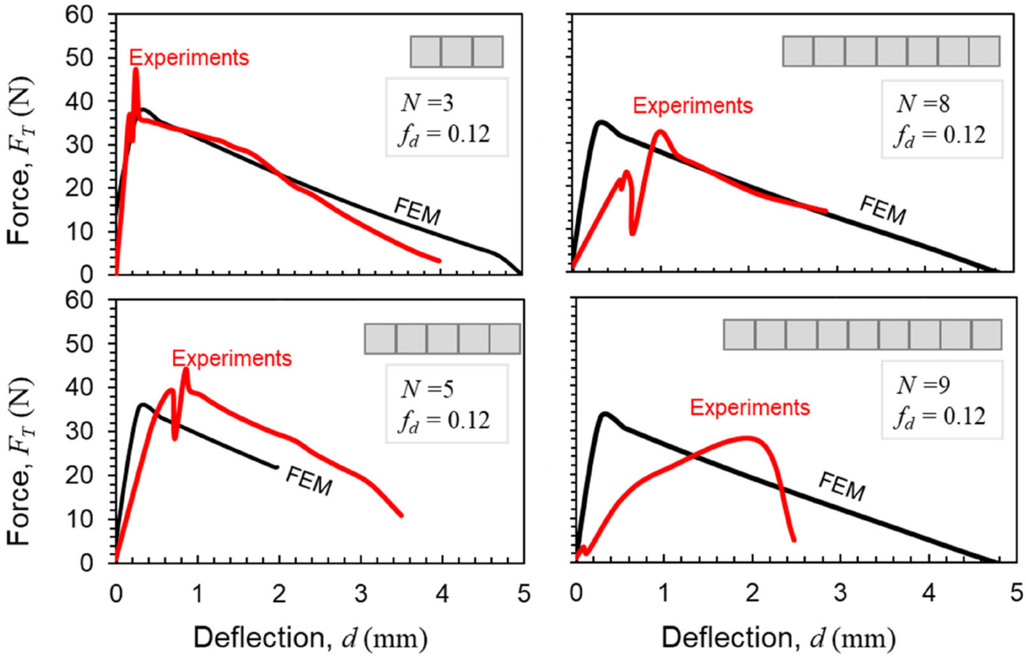

Figure 5. $F_T - d$ responses from experiments (red) compared with FEM simulations (black) for $N = 3$, 5,7, and 9.

a sharp linear increase until the onset of sliding $F_T^{(s)}$. Beyond this point, the blocks began to slide, causing the compressed elastic volume to decrease[5,29]. Consequently, the sliding force F_T decreased almost linearly until the displaced block lost contact with its neighboring blocks. At this stage, the axial compression vanishes, and the static equilibrium was lost. The deformation prior to sliding followed the simple analytical expression derived in Ref.[5]:

$$\frac{F_T^{(s)}}{F_A} = \frac{16f}{3\left(4 + f^2(N-2)^2\right)} \quad 0 < d < d_s \tag{8}$$

where the subscript s denotes the onset of sliding. First, for $N = 3$ and $f = 0.18$, the onset of sliding predicted from Eq. (1), $F_T^{(s)} = 35.7$ agrees with the numerical simulation results within 4% (Fig. 4). Thus far, Eq. (1), and the simulations verified each other. In the post-sliding regime, the sliding force for d >ds can be expressed using Ref.[5]:

$$\frac{F_T}{F_A} = 2f\left(1 - \frac{d}{L}\right) \quad d_s < d < L \tag{9}$$

This explains the observed linear decline. Equation (1) describes the reduction in the onset of sliding as the number of blocks N increases.

Figure 4 shows the axial stress σ_{xx} normalized by the maximum axial stress. The highest stress occurred at the leading edge of the sliding interface, where the edge was sharpest.

Segmentation at low block numbers breaks the beam into discrete interfaces, causing the system to behave more like a granular assembly than a homogeneous continuum. Importantly, for a brittle counterpart, such as a glass beam, the segmented configuration makes the system predictable, as demonstrated by both simulations (Figure 4) and simple Euler-based expressions (Eqs. (1)–(2)). Significantly, segmentation endows an otherwise brittle system with ductility; the resulting beam can deform smoothly and dissipate energy through friction[30] instead of failing suddenly through a catastrophic fracture, in which the stored energy is released as fracture noise and the dynamic spread of glass fragments.

3.3. Experimental Verification of the Model.

Once we developed a basic understanding of the transverse loading response of the segmented beams, the FEM model introduced above was validated experimentally. Existing literature contains several measurements of segmented beam deformation and their corresponding force–deflection curves[5]. We extracted the raw experimental data for the same segmented beam setup shown in Figure 6 and the same friction coefficient values from Ref.[5]. The experimental data are represented by a red curve. Using the same parameters reported in these experiments: $f = 0.18$, $N = 3$-9, $F_A = 150\,\mathrm{N}$, and $E = 1.48\,\mathrm{GPa}$, we ran simulations and compared the results with the experimental data shown in Fig. 5.

For $N = 3$, the FEM prediction (black curve) closely follows the experimental response (red curve). For $N = 5$, the FEM also captured the experimental trend but with slightly larger deviations. For $N = 7$ and $N = 9$, the FEM predicted a graceful sliding deformation, whereas the experiments showed the same deformation mode, but with a noticeably smaller response. In the experiments, the initial linear rise (elastic region) was lower than that in the simulations, and the subsequent behavior exhibited a parabolic-like decline, indicating significant softening as the stiffness decreased.

This softening suggests that the segmented beam entered an elastic deformation regime dominated by the geometric jamming of the blocks, causing the system to behave like a standing truss, where the increased transverse load stores more elastic energy. Overall, the FEM model captured the essential physics of the segmented beam accurately, although the deviation increased as the number of blocks N became larger.

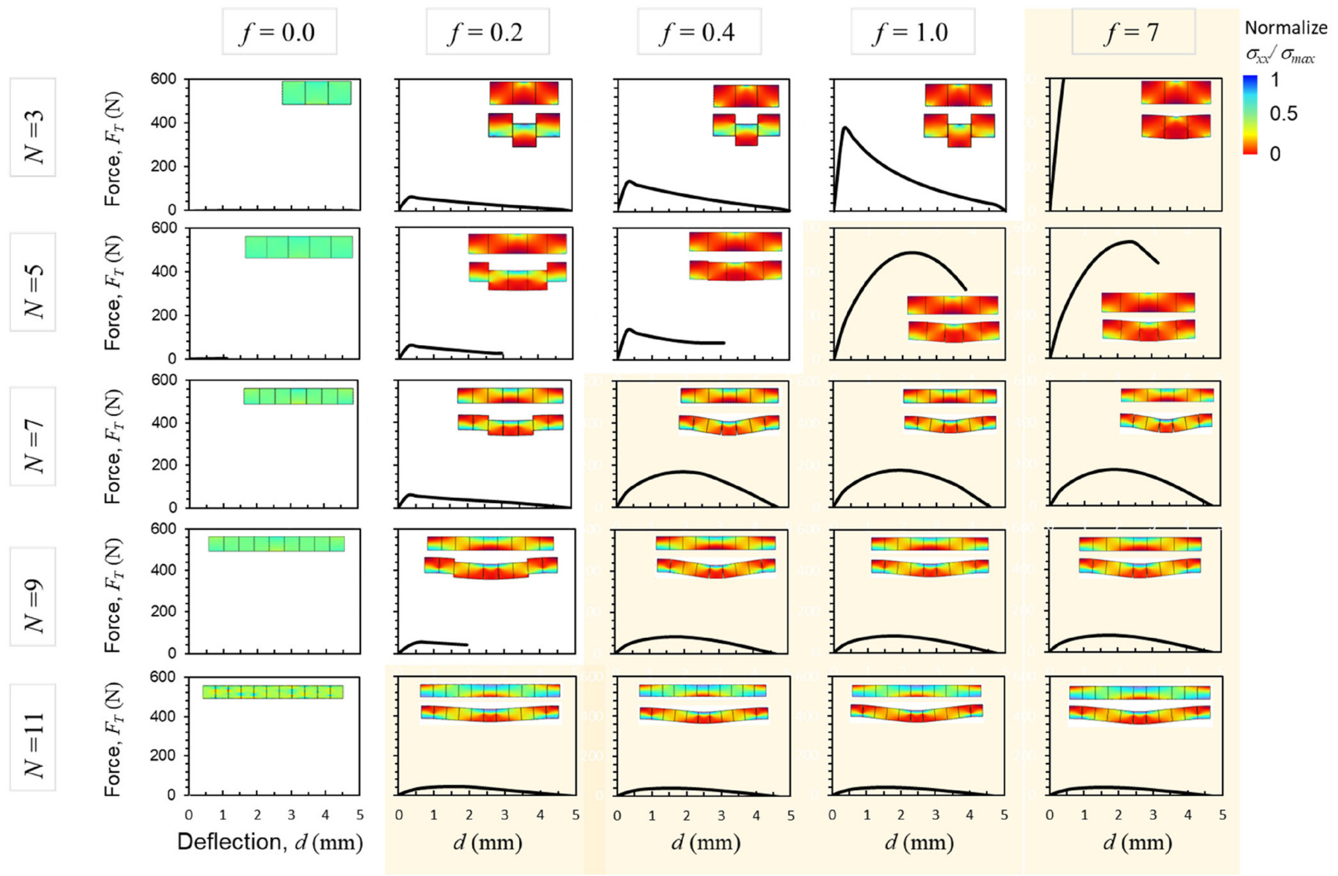

Figure 6. $F_T - d$ responses based on the FEM;, $N = 3, 5, 7, 9$ and 11 and friction coefficients; and $f = 0, 0.2, 0.4, 1.0$, and 7.0.

3.4. Beam Structure as a Material. Once the FEM model was verified and validated experimentally, we proceeded with a computational sweep over the parameter design space (N,f). We ran the FEM for $f = 0, 0.2, 1.0$, and 7, from low friction to extreme levels, and for $N = 3, 5, 7, 9$, and 11 blocks, using the same elastic and axial force parameters as before. Figure 6 shows all the force–deflection plots ($F_T - d$) for the above-mentioned parametric sweep. For the frictionless cases $(f = 0)$, as shown in the first column, the solver registered extremely low forces near the machine zero $\sim 10^{-13}$ N, and thus, the system was unstable and the solver could not proceed except for a few pseudo increments. Therefore, without friction, the segmented beam could not maintain its stability and had no load-bearing capacity (Fig. 6). In Fig. 6, the insets of each plot show the undeformed and deformed beams.

With increased friction, i.e., the second column for $f = 0.2$, the segmented array exhibited a linear increase and onset of sliding, followed by sliding until loss of bearing capacity (as in Fig. 4) only for the case of 3–9 blocks. With an increased number of blocks ($N > 9$), the array transitioned into another mode of deformation where the blocks bent like a continuous beam, characterized by the tendency of the interfaces to open due to block rotation, which we called "hinging" as per Ref.[5]. This mode was also characterized by a gradual softening in stiffness during deformation (the slope of the force–deflection curve), showing a parabolic trend. One major difference is that the area under the curve (AUC), which visualizes the absorbed energy, is predominantly due to the elastic energy built into the structure. The structure acted more like a continuous beam but with enhanced deformation (more compliant). Thus, the structure lost its energy-dissipation mechanism. The regions characterized by the hinging mode are highlighted with an orange background in the grid in Fig. 6.

With a further increase in the number of blocks ($N = 9$ and 11), the tendency of the interfaces to open diminished, and the segmented beam began to exhibit the behavior of a continuous beam. In other words, the segmented beam structure began to behave as a homogeneous continuum for $N > 11$at $f = 0.2$. At $f = 0.4$, the sliding persisted up to $N = 5$. For larger numbers of blocks, $N > 5$, parabolic hinging-mode deformation emerged, and the tendency of the interfaces to open ceased around $N \geq 9$. By increasing the friction to extreme levels, such as $f = 1.0$ and 7, sliding was only observed at $N =$ 3for $f = 1.0$, and the structure exhibited only hinging for $f = 7$. For $f = 1.0$, the tendency of interface opening ceased for $N \geq 7$, and for $f = 7$ it ceased already at $N \geq 3$. Thus, it is reasonable to suggest that for $f > 7$, the material interfaces act as fused blocks, and the system behaves more like a continuous beam (i.e., approaching a continuum) without the homogenization of its apparent properties. In this regime, the segmented beam transitions from discrete granules (i.e., individual blocks) to continuum-like behavior, where the interfaces remain intact and the stiffness modulation is preserved across scales. Maintaining the advantage of interfaces is important for ensuring crack resistance because cracks are forced to deflect along these interfaces[4,17].

In summary, segmented structures can be transitioned, at least for the beam case presented herein, via increased friction or an increased number of blocks. Both are analogous to interatomic bonding and increase the number of units (i.e., separation of scale) in lattice materials and composites[16]. Increased friction also caused the maximum traverse force to increase. Therefore, both the strength and stiffness of the beam increased with friction. An increase in N softens the beam and decreases its strength. Increasing both N and f promotes hinging over sliding and makes the beam structure behave more like a continuous beam.

4. CONCLUSION

This study introduced the mechanics of segmented beams and established their basic transverse responses, including the linear regime, sliding onset, and post-sliding behavior. The FEM model was further validated against existing experiments and captured the main deformation modes, with deviations increasing only for larger values of N. With the model verified, a parametric study of (N and f) showed that friction stabilized the segmented beam and increased its strength and stiffness, whereas an increase in N softened the beam and decreased its strength. High friction or N suppressed sliding and promoted hinging, causing the segmented beam to behave more like a continuous beam, effectively transitioning from a structure to a continuum. This behavior is analogous to increased bonding or scale separation in lattice materials and composites. Despite these findings, this study has several limitations that should be acknowledged. The model is developed under quasi-static conditions, meaning that dynamic and rate-dependent effects are not considered; therefore, the results are most applicable to slow loading scenarios. Friction between blocks is represented using a simplified Coulomb model with equal static and dynamic coefficients, which does not capture more complex behaviors such as stick–slip transitions or surface wear. In addition, the analysis focuses on a segmented beam configuration, selected as a simple and well-understood system to isolate the key mechanics; consequently, extending these findings to more complex geometries or fully three-dimensional architectured materials should be done with caution. Finally, the conclusions are based on a specific parameter space defined by block number and friction coefficient; while they provide useful mechanistic insight, they are not intended to be universally applicable to all segmented systems.

AFFILIATIONS AND AUTHOR DETAILS

Undergraduate Author

Mohannad F. Al Sindhi – *Undergrad student, Bioengineering Department, King Fahd University of Petroleum & Minerals, Dhahran 31261, Saudi Arabia;* 0009-0009-6646-3060
Email: s202277320@kfupm.edu.sa

Corresponding Author

Ahmed S. Dalaq – *Research Mentor, Assistant Professor, Bioengineering Department, King Fahd University of Petroleum & Minerals, Dhahran 31261, Saudi Arabia & IRC for Biosystems and Machines, King Fahd University of Petroleum & Minerals, Dhahran 31261, Saudi Arabia;* 0000-0002-3070-4215
Email: ahmed.dalaq@kfupm.edu.sa

ACKNOWLEDGEMENTS

This work was supported by the IRC for Biosystems and Machines at King Fahd University of Petroleum and Minerals (KFUPM), Saudi Arabia.

DATA AVAILABILITY

Data will be made available upon request

REFERENCES

(1) Davis, G. K. & Patel, N. H. The origin and evolution of segmentation.

(2) Lloyd, C. *et al.* Hydrodynamic efficiency in sharks: the combined role of riblets and denticles. *Bioinspir. Biomim.* **16**, (2021).

(3) Owner, P. B. Giant shark spine found in Bournemouth – species revealed. *Practical Boat Owner* https://www.pbo.co.uk/news/giant-shark-spine-found-in-bournemouth-species-revealed-70525 (2022).

(4) Barthelat, F. Architectured materials in engineering and biology: fabrication, structure, mechanics and performance. *Int. Mater. Rev.* **60**, 413–430 (2015).

(5) Dalaq, A. & Barthelat, F. Strength and stability in architectured spine-like segmented structures. *Int. J. Solids Struct.* **171**, Pages 146-157 (2019).

(6) Oxland, T. R. Fundamental biomechanics of the spine—What we have learned in the past 25 years and future directions. *J. Biomech.* **49**, 817–832 (2016).

(7) Dunn, I. F. Lumbar spine injuries in athletes. *Neurosurg Focus* **21**, (2006).

(8) Porter, M. E., Ewoldt, R. H. & Long, J. H. Automatic control: the vertebral column of dogfish sharks behaves as a continuously variable transmission with smoothly shifting functions. *J. Exp. Biol.* **219**, 2908–2919 (2016).

(9) Estrin, Y., Dyskin, A. V. & Pasternak, E. Topological interlocking as a material design concept. *Mater. Sci. Eng. C* **31**, 1189–1194 (2011).

(10) Estrin, Y., Dyskin, A. V., Pasternak, E., Khor, H. C. & Kanel-Belov, A. J. Topological interlocking of protective tiles for the space shuttle. *Philos. Mag. Lett.* **83**, 351–355 (2003).

(11) Dyskin, A., Estrin, Y. & Pasternak, E. Topological Interlocking Materials. in *Architectured Materials in Nature and Engineering Archimats* (eds Estrin, Y., Brechet, Y., Dunlop, J. & Fratzl, P.) 23–49 (Springer, Switzerland, 2019).

(12) Aravinthan, T., Karunasena, W. (Karu) & Wang, H. *Futures in Mechanics of Structures and Materials: Proceedings of the 20th Australasian Conference on the Mechanics of Structures and Materials (ACMSM20), Toowoomba, Australia, 2-5 December 2008.* (CRC Press, London, United Kingdom, 2009).

(13) Mechanics A. C. on A. *et al. Applied Mechanics: progress and applications, proceedings of the third Australasian Congress on Applied Mechanics, Sydney, Australia, 20-22 February 2002.* (World Scientific, 2002).

(14) Dyskin, A. V., Estrin, Y., Kanel-Belov, A. J. & Pasternak, E. A new concept in design of materials and structures: assemblies of interlocked tetrahedron-shaped elements. *Scr. Mater.* **44**, 2689–2694 (2001).

(15) Dyskin, A. V., Estrin, Y., Kanel-Belov, A. J. & Pasternak, E. Toughening by Fragmentation—How Topology Helps. *Adv. Eng. Mater.* **3**, 885 (2001).

(16) Ashby, M. F. & Bréchet, Y. J. M. Designing hybrid materials. *Acta Mater.* **51**, 5801–5821 (2003).

(17) Mirkhalaf, M., Tanguay, J. & Barthelat, F. Carving 3D architectures within glass: Exploring new strategies to transform the mechanics and performance of materials. *Extreme Mech. Lett.* **7**, 104–113 (2016).

(18) Wadley, H. N. G. *et al.* Effect of core topology on projectile penetration in hybrid aluminum/alumina sandwich structures. *Int. J. Impact Eng.* **62**, 99–113 (2013).

(19) Mirkhalaf, M. & Barthelat, F. Design, 3D printing and testing of architectured materials with bistable interlocks. *Extreme Mech. Lett.* **11**, 1–7 (2017).

(20) Siegmund, T., Barthelat, F., Cipra, R., Habtour, E. & Riddick, J. Manufacture and Mechanics of Topologically Interlocked Material Assemblies. *Appl. Mech. Rev.* **68**, 040803 (2016).

(21) Khandelwal, S., Siegmund, T., Cipra, R. J. & Bolton, J. S. Transverse loading of cellular topologically interlocked materials. *Int. J. Solids Struct.* **49**, 2394–2403 (2012).

(22) Dyskin, A. V., Estrin, Y., Kanel-Belov, A. J. & Pasternak, E. Topological interlocking of platonic solids: A way to new materials and structures. *Philos. Mag. Lett.* **83**, 197–203 (2003).

(23) Dalaq, A. S. & Barthelat, F. Manipulating the geometry of architectured beams for maximum toughness and strength. *Mater. Des.* **194**, 108889 (2020).

(24) Kim, D. Y. & Siegmund, T. Chirality in topologically interlocked material systems. *Mech. Mater.* **191**, 104956 (2024).

(25) Laudage, S., Guenther, E. & Siegmund, T. Design and analysis of a lightweight beam-type topologically interlocked material system. *Structures* **51**, 1402–1413 (2023).

(26) Ugural, A. C. & Fenster, S. K. *Advanced Mechanics of Materials and Applied Elasticity*. (Pearson Education, 2011).

(27) Zavarise, G., Wriggers, P. & Schrefler, B. A. On augmented Lagrangian algorithms for thermomechanical contact problems with friction. *Int. J. Numer. Methods Eng.* **38**, 2929–2949 (1995).

(28) COMSOL, A. COMSOL Multiphysics®v. 6.3. COMSOL AB (2024).

(29) Dalaq, A. S., Mirkhalaf, M. & Barthelat, F. Strength, stability, and interlocking efficacy in topologically interlocked materials based on tetrahedra and octahedra. *Int. J. Solids Struct.* **321**, 113575 (2025).

(30) Garland, A. P. *et al.* Coulombic friction in metamaterials to dissipate mechanical energy. *Extreme Mech. Lett.* **40**, 100847 (2020).